THE JOURNAL OF
PHYSICAL CHEMISTRY B

Single-Cell Mechanics Provides an Effective Means To Probe in Vivo Interactions between Alveolar Macrophages and Silver Nanoparticles

Ying X. Liu,[†] Arpad Karsai,[†] Donald S. Anderson,[‡] Rona M. Silva,[‡] Dale L. Uyeminami,[‡]
Laura S. Van Winkle,[‡,§] Kent E. Pinkerton,[‡,§,∥] and Gang-yu Liu*,[†]

[†]Department of Chemistry, [‡]Center for Health and the Environment, [§]Department of Anatomy, Physiology and Cell Biology, School of Veterinary Medicine, and [∥]Department of Pediatrics, School of Medicine, University of California, Davis, California 95616, United States

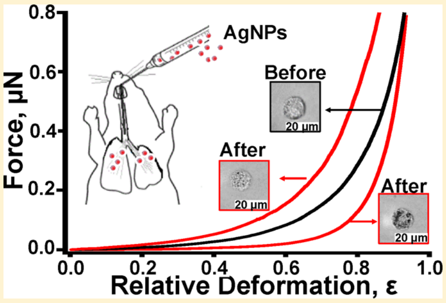

ABSTRACT: Single-cell mechanics, derived from atomic force microscopy-based technology, provides a new and effective means to investigate nanomaterial−cell interactions upon in vivo exposure. Lung macrophages represent initial and important responses upon introducing nanoparticles into the respiratory tract, as well as particle clearance with time. Cellular mechanics has previously proven effective to probe in vitro nanomaterial−cell interactions. This study extends technology further to probe the interactions between primary alveolar macrophages (AM) and silver nanoparticles (AgNPs) upon in vivo exposure. Two types of AgNPs, 20 and 110 nm, were instilled to rat lung at 0.5 mg AgNPs/kg body weight, and allowed 24 h interaction. The consequences of these interactions were investigated by harvesting the primary AMs while maintaining their biological status. Cellular mechanics measurements revealed the diverse responses among AM cells, due to variations in AgNP uptake and oxidative dissolving into Ag^+. Three major responses are evident: zero to low uptake that does not alter cellular mechanics, intracellular accumulation of AgNPs trigger cytoskeleton rearrangement resulting in the stiffening of mechanics, and damage of cytoskeleton that softens the mechanical profile. These effects were confirmed using confocal imaging of F-actin and measurements of reactive oxygen species production. More detailed intracellular interactions will also be discussed on the basis of this study in conjunction with prior knowledge of AgNP toxicity.

■ INTRODUCTION

Silver nanoparticles (AgNPs) have sparked an increasing demand for high throughput production and are being used widely in consumer product applications,[1,2] medical use,[3] and cloud seeding.[4] The increased inhalation exposure to AgNPs in occupational settings,[4] as well as in daily life,[2] has raised concerns about potential acute and chronic health impacts following their entry into human body.[5] Toward this direction, alveolar macrophage−nanoparticle (NP) interactions represent the initial and critical steps in pulmonary responses to exogenous particulates, therefore attracting much attention.[1−8]

In vivo studies using animal models have shown that entry of silver nanoparticles (AgNPs) into the respiratory tract can induce acute pulmonary inflammation and chronic lung damage.[6,8,9] In the case of acute responses, macrophages migrate to sites of NP deposition in the lung parenchyma. This occurs even upon a single exposure to AgNPs.[8,10] Macrophages could intake AgNPs via endocytosis,[11,12] phagocytosis via scavenger receptors,[8,13] or direct entry.[14] One consequence is the release of inflammatory mediators, such as cytokines and reactive oxygen species (ROS).[8,12,13,15,16] These macrophage−NP interactions often produce acute pulmonary inflammation.[8,17] NPs may also produce frustrated phagocytosis among macrophages leading to cell death.[15] In the case of chronic responses, substances released by macrophages can lead to subsequent inflammation[15] and changes in lung structure, such as granulomatous lesions and thickened alveolar walls.[18]

To understand the mechanism and consequence of AgNPs' interactions with macrophages, in vitro assays have been completed with RAW264.7 (mouse macrophage) and NR8383 (rat alveolar macrophage) cell lines.[13,19] These in vitro studies have the advantages of screening a high number of cells with high reproducibility, and being free of animal use. In vitro assays have provided important insights regarding NP−cell interactions. For example, AgNPs were found to trigger inflammatory responses, increase ROS production, and induce cell death in a dose-dependent manner upon in vitro exposure.[7,11,13,19−21] In vitro studies have also found smaller AgNPs, such as 15, 20, and 35 nm AgNPs, to be more toxic than the larger ones, such as 55 or 110 nm NPs.[13,19,20]

Despite informative studies, in vitro assays are frequently questioned and challenged regarding their relevance to in vivo nanotoxicology.[22,23] The basis of these challenges originates from the fact that in vitro studies could not effectively mimic in vivo NP−cell interactions. For example, physicochemical properties of NPs in the culture media in vitro could differ from those in vivo. One outcome is the protein coronas that

Received: August 6, 2015
Revised: November 9, 2015
Published: November 12, 2015

DOI: 10.1021/acs.jpcb.5b07656

form when nanomaterials contact the mucous lining layer of the lung.[24,25] To attain measurable responses, in vitro doses are typically much higher than those given in vivo; thus, local concentrations of NPs in culture media could be higher than in the animal lung.[26,27] Further, the monoculture systems and unnatural uniformity of in vitro assays may not effectively mimic multiple cell types and heterogeneity inside animal lungs.[28] Finally, the possible interference of NPs with assay reagents also raises concerns regarding the reliability of in vitro assays.[29]

To address these challenges, primary alveolar macrophages (AM) from unexposed animals have been used for in vitro exposures and assays.[7] Utilization of primary cells brought these measurements a step closer to in vivo relevancy. However, this approach still could not effectively mimic the complexity of in vivo exposure. One difficulty is the heterogeneity and variation in the local environment in vivo, which could not be effectively investigated using in vitro biochemical assays, where the exposures are relatively similar among cells, and the outcome is based on the average responses of the 10^4–10^6 cells.[8] Single-cell-based methods in conjunction with primary cells upon in vivo exposure could bring us one more step closer to addressing the challenges.

Atomic force microscopy (AFM) technique has been widely used to quantify nanomechanical properties in living cells and biological materials.[30−40] However, most AFM-based mechanical measurements probe local mechanics and are therefore highly dependent on probe size and targeting position and require multiple curves to map the mechanical properties of the whole cell.[35] An AFM-based method was developed by our team that offers a single-cell-based readout toward this requirement.[41] The concept is illustrated in Figure 1. A cell is compressed under a spherical probe, while the deformation and corresponding forces are simultaneously recorded and monitored. Cellular mechanics are known to be sensitive to the changes in the biological status of cells.[31,42,43] Our prior work demonstrates the capability and sensitivity of single-cell mechanics to reveal cellular membrane stiffening with a cell tracing dye at below normal dosage, and distinctive responses to the aggregation forms of amyloid β peptide.[41,44,45] Cell mechanics measurements have also been shown to be sensitive to interactions between NPs and living human aortic endothelial cells (HAEC) following in vitro exposure.[46] Results show that ZnO NPs stiffen the membrane and cause ion flux dysfunction, and eventually inflammation at the low concentration of 10 μg/mL, whereas SiO_2 NPs appear benign in HAEC.[46] The current work takes single-cell mechanics studies one step further to explore the feasibility, advantages, and limitations as a readout for AgNP−pulmonary AM interactions following in vivo exposure to the respiratory tract through intratracheal instillation (IT), a technique commonly used in lung toxicity studies.[47] Because the focus of this study is to test the effectiveness of our approach in revealing NP−AM interactions upon in vivo exposure, we adopt the previously established IT protocols over inhalation to attain quantitative and consistent dosage.[47−49] Measurements at the single-cell level after in vivo exposure shall provide a better understanding of the heterogeneity of AM responses to NPs. This approach also has potential to establish correlation of the cytotoxicity between in vitro and in vivo systems.

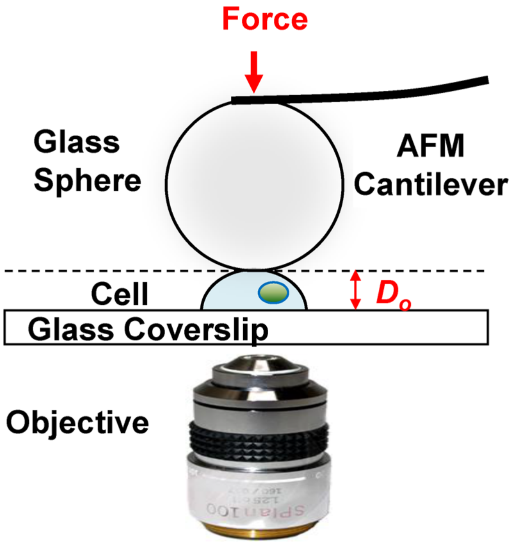

Figure 1. Schematic diagram to illustrate atomic force microscopy-based single-cell compression concept.

EXPERIMENTAL METHODS

Silver Nanoparticles. AgNPs (NanoComposix, San Diego, CA, USA) utilized in this study were supplied by the National Institute of Environmental Health Sciences Centers for Nanotechnology Health Implications Research (NCNHIR) consortium and characterized by dynamic light scattering and transmission electron microscopy.[50,51] Two sizes of AgNPs, 20 and 110 nm, were supplied as 1 mg/mL stock suspensions in 2 mM citrate buffer. Stock suspensions were diluted in 2 mM citrate buffer to reach 0.5 mg/mL for instillation studies. Two millimolar citrate buffer, pH 7.5, was prepared by dissolving trisodium citrate dehydrate (Sigma, St. Louis, MO, USA) in endotoxin free water (Fisher Scientific, Hanover Park, IL, USA). AgNP stock suspensions were sonicated for 5 min, to break up aggregates immediately prior to use/dilution.

AgNP Characterization. AFM measurements were performed on a MFP-3D AFM (Asylum Research, Santa Barbara, CA, USA). Silver nanoparticle (1 mg/mL) suspensions were immobilized on a 0.1% (w/v) poly-L-lysine (P8920, MW 150 000−300 000 Da, Sigma, Saint Louis, MO, USA)-coated mica (0001) surface. Sharpened silicon cantilevers (AC240, Olympus) were used for imaging. Images were acquired using tapping mode in air. The imaging speed was 5.0 μm/s. The driving frequency was set at the fundamental resonance of the cantilever, typically 75 kHz. The imaging set point was adjusted to 75% damping of the free amplitude.

In vivo Exposures Using Animal Models. The animal study was performed under protocols approved by the University of California Davis IACUC in accordance with National Institutes of Health guidelines. Intratracheal instillation and harvesting of AMs followed established protocols.[47,51−53] Briefly, 12 week old male Sprague−Dawley (SD) rats (Harlan Laboratories, Hayward, CA, USA) were acclimated for 1 week prior to treatment. The animals were anesthetized with 3% isoflurane via a Quantiflex anesthesia unit (Medmark Crop., Versailles, OH, USA) and intratracheal instillations were carried out with 0.5 mg/kg body weight (b.w.) of AgNPs and 350 μL total volume. A total of 26 rats were used in this study. The number of rats used per exposure was 10 and 8 for AgNP1 and AgNP2, respectively, and we ran at least 4 sets for each condition at different days. To examine the true impact of Ag ions on cellular mechanics, $AgNO_3$ was dissolved in endotoxin free water and was used at a dosage of 0.05 mg/kg b.w. typically with 2 rats per instillation condition. For each experiment, we designated one rat into which only 350 μL of 2 mM citrate buffer was instilled. Citrate buffer instillation serves as a good control because this buffer solution has little impact on acute pulmonary responses.[49−51,54] Further, reference instillation must be performed to extract the impact of AgNPs which disperse into the citrate buffer media.

Twenty-four hours after instillation, the animals were necropsied and AMs were collected by bronchoalveolar lavage (BAL) from the right lobe of each lung by washing with the same 8 mL of prewarmed 0.9% sterile saline three times. Bronchoalveolar lavage is proven to be an adequate and informative technique that can give valuable insight into inflammatory processes of the lung[55] by harvesting cells from the alveoli and airways. The method is widely used in human medicine to establish diagnosis on the pathological features of the collected sample.[55] The main factor to have successful lavage and to remove the cells in the epithelial lining fluid of the lung is the amount of used lavage fluid. Our prior studies demonstrated that 8 mL of saline solution three times washing of rat lung produced excellent results.[53] By using this high volume lavage protocol to collect BALF, we made sure that the collected cells represent the cell population being present in the alveoli of examined rats.

Cells were collected and excessive AgNPs from BALF were removed by centrifugation of the BALF at 2000 rpm at 4 °C for 10 min. This level of centrifugation causes cells to pellet, but AgNPs not internalized by cells remain in suspension. Cells were again suspended, maintained in fresh physiological saline solution, and placed on ice to prevent further AgNP uptake during BALF collection and transportation.

Macrophage Cell Preparation for Single-Cell Mechanics Measurements. Upon receipt of BALF, precautions were taken to ensure purity and high population of AMs for single-cell mechanics measurements. Cells derived from BALF consist predominantly of neutrophils [polymorphonuclear leucocytes (PMNs)], and alveolar macrophages (AMs), as determined by cytospin staining.[49] Because PMNs are much less adherent to glass than are AMs, they can be mostly removed by immobilization on the glass substrate and subsequent washing steps. Therefore, cells were first suspended in Roswell Park Memorial Institute (RPMI) 1640 medium containing 10% fetal bovine serum (Gibco, Grand Island, NY, USA), and then most AMs were allowed to adhere to the glass bottom of a MatTek dish (MatTek, Ashland, MA, USA) for 1−1.5 h at 37 °C in a 5% CO_2 humidity incubator. The dish was washed using medium to remove loosely bound PMNs. The attachment and washing could be repeated if needed to increase the purity of AMs. The purity of the sample was verified by optical microscopy because macrophages are twice the size as leukocytes. Prior to single-cell mechanics measurement, fresh medium was introduced.

Optical Microscopy and Simple Quantification of Darkness Score. The level of dark optical contrast of individual AM was quantified using ImageJ on optical images captured under a 60× objective during the cell compression process. These images were recorded by a CCD camera that detects only the intensity of the sample and produces a gray scale image (Sony) coupled with GrabBee software (Video-Home Technology Corp.) and are displayed at a gray scale from 0 to 255, where 0 represents the darkest color and 255 represents the whitest color. Under optimal focus and same setting of optical microscopy, the degree of dark contrast, defined as darkness, was calculated via

$$\begin{aligned}\text{darkness score} = (&\text{area of dark features within selected cell}\\ &\times \text{mean grey value of background readings}\\ &- \text{integrated density})/10000 \qquad (1)\end{aligned}$$

Cells with a score below 7 are considered to have low darkness, whereas a score above 21 is considered high darkness. Medium darkness is between 7 and 21. The low darkness threshold is double the maximum darkness value of the control cells to compensate for the uncertainty of optical microscopy measurement, whereas the high darkness threshold is set to be triple the low darkness threshold and reflects the optical contrast where actin network damage occurred upon AgNP exposure.

Single-Cell Mechanics Measurements. Atomic force microscopy-based single-cell compression was developed by our team and reported previously.[41] Briefly, a cell is compressed between a modified AFM spherical probe and the glass substrate, as illustrated in Figure 1. A soft silicon cantilever (AC240, spring constant of 1−2 N/m, Olympus America, Center Valley, PA, USA) was modified by attaching a 40 ± 2 μm glass sphere to apex of the AFM tips using a premixed two-component epoxy (S-31, ITW Performance Polymers, Riviera Beach, FL, USA). Our goal is to probe the mechanics of an entire cell instead of local or regional mechanics within the cell. Therefore, the glass sphere must be sufficiently large to probe the responses from the entire cell during compression. On the contrary, we hope to use spheres as small as possible to gain a good view of cells during experiments. Empirically, the diameter must be much larger than the cellular height. To ensure detection from the entire AM cell underneath, we tested spheres with diameter ranging from 20 to 100 μm and found that the 40 μm glass spheres are sufficiently large.[41,45,46] To ensure the fidelity of the single-cell mechanics to reflect the entire cell in response to treatment, we only reported the compression cycle of cell upon the first compression above the center. The actual spring constant of the modified AFM probe was measured and quantified using the added mass method[56] and corrected with respect to the probe position.[57] Force deformation profiles of cells were measured with a MFP-3D AFM (Asylum Research Corp., Santa Barbara, CA, USA). The AFM was combined with an inverted optical microscope (IX50, 60× objective, Olympus America, Center Valley, PA, USA) under bright field illumination to guide alignment of the modified AFM probe with respect to the target cell. Prior to each single-cell compression, cells were inspected via optical microscopy to ensure the representative populations were selected. The morphology of the cell was monitored during the compression cycle via optical microscopy.

Force-deformation profiles were first acquired on a glass substrate nearby to establish an internal reference and force profile for cell height calculation. Each cell was compressed once at the apex of the cell as the deformation profile was recorded. The compression was performed at a relatively low rate of 2 μm/s to prevent hydrodynamic contributions.[41] All cell compression experiments were restricted to less than 40 min in culture medium with 5% CO_2 atmosphere. Individual cell viability was confirmed before seeding and after cell mechanics measurement using trypan blue stain (21 μM, Invitrogen, Carlsbad, CA, USA) as described previously.[41,46] The cells were confirmed to be >95% viable.

Table 1. Single-Cell Mechanics Measurements of AMs in Conjunction with Results from Optical Imaging upon in Vivo Exposure to AgNPs

treatment and abbreviation	single-cell mechanics	cells selected	height (μm)	volume (μm^3)	darkness (au)	F (nN) @ $\varepsilon = 0.3$	F (nN) @ $\varepsilon = 0.6$	E_m (MPa)	E_c (kPa)
citrate buffer (CAM)	unchanged	13	12.9 ± 1.3	2314 ± 573	1.4 ± 1.0	30.4 ± 16.0	156 ± 61	1.1 ± 0.5	5.9 ± 2.7
AgNP1 in citrate buffer (AgNP1-CAM)	stiffer	3	13.7 ± 1.6	2495 ± 629	6.3 ± 7.9	**62.3 ± 18.7**	**288 ± 46**	1.1 ± 0.6	**12.5 ± 6.9**
	unchanged	8	12.2 ± 1.6	2098 ± 613	7.0 ± 6.3	24.9 ± 7.8	162 ± 36	1.2 ± 0.5	6.0 ± 2.7
	softer	8	12.9 ± 1.3	2153 ± 479	18.0 ± 20.4	**7.2 ± 4.6**	**48 ± 20**	**0.3 ± 0.2**	**2.2 ± 1.2**
AgNP2 in citrate buffer (AgNP2-CAM)	stiffer	3	14.8 ± 1.1	3135 ± 698	2.0 ± 0.6	**86.8 ± 12.1**	**324 ± 26**	1.2 ± 0.4	**19.2 ± 6.3**
	unchanged	7	12.4 ± 0.8	2239 ± 528	10.2 ± 13.6	18.4 ± 5.6	110 ± 23	1.1 ± 0.5	3.5 ± 1.2
	softer	8	13.5 ± 1.4	2587 ± 578	14.2 ± 11.6	**6.2 ± 2.1**	**40 ± 13**	**0.3 ± 0.2**	**1.1 ± 0.6**
0.05 mg Ag^+/kg (Ag^+(0.05))	stiffer	6	16.8 ± 0.5	4773 ± 418	1.5 ± 1.0	**55.1 ± 15.5**	**222 ± 45**	0.9 ± 0.6	7.2 ± 1.6

Because cell shapes remain similar, the profiles are displayed as force vs relative deformation (ε).[41,46] Relative deformation, ε, is defined as change in cell height (Δz) over the initial uncompressed cell height (D_0). The cell volume was calculated using lateral measurements taken from optical images of cells on the substrate and from initial cell height measured by AFM. The cell shape was modeled as a spherical cap.[45]

Calculation of Membrane Young's Modulus from Cellular Mechanics Measurements. To quantify Young's modulus of cellular membrane (E_m) and cytoskeleton (E_c) from force profiles, cells were approximated as balloons containing liquid.[41,45,46,58] Hertzian contact mechanics were adapted to allow analytical quantification of force profiles under relatively low deformation, where the assumptions remain valid.[41] When the balloon is compressed between two parallel plates, the force-deformation follows a cubical relationship for the membrane, whereas the cytoskeleton contribution follows a different power law (3/2), as shown in eq 2:

$$F = F_m + F_c = 2\pi\frac{E_m}{1 - \nu_m}hR_0\varepsilon^3 + \frac{\sqrt{2}E_c}{3(1 - \nu_c^{\ 2})}R_0^{\ 2}\varepsilon^{3/2} \tag{2}$$

where ε is relative deformation of the cell, R_0 and h are the radius of the uncompressed cell and membrane thickness, respectively, ν_m and ν_c represent Poisson ratios of membrane and cytoskeleton, respectively, and E_c and ν_c represent the Young's modulus and the Poisson ratio of cytoskeleton. At relatively small deformation and before cellular damage, this equation remains valid and one could quantify the E_m.[41,44−46,59] The two Poisson ratios, $\nu_m = 1/2$ and $\nu_c = 0$, respectively, mean cells remain nonpermeable during the full range of compression. The cellular diameter, D_0, can be measured from AFM imaging as well as cellular compression, from which radius can be determined, $R_0 = 0.5D_0$. For most cells, $h = 4$ nm. Therefore, least-squares fitting of the force-deformation profiles using eq 2 allows quantification of E_m and E_c in one step.[41,44−46,58]

Osmotic Pressure Quantification. Given the swelling due to direct instillation of Ag^+, ion flux dysfunction is expected to have occurred.[45,46] Assuming the observed left-shift is solely due to ion flux dysfunction, the change in intracellular ion concentration (ΔC) can be estimated from force vs ε profiles using the following method reported previously:[45] Briefly here, the increase in osmotic pressure could be estimated using the force vs ε profile following eq 3

$$\Delta F = \Pi \cdot S \tag{3}$$

where ΔF, Π, and S are force difference between the selected cell in comparison to the corresponding control cell at given deformation, osmotic pressure increase, and cell-probe contact area, respectively. The contact area, S, between the glass probe and the hemispherical cell at the small deformation can be estimated following eq 4:

$$S = 2\pi R^2\varepsilon \tag{4}$$

where R is the contact radius, and it equals cell height in this approximation.

With the known ΔF and S for a target cell, ΔC can be calculated using the following eq 5 from the osmotic pressure−ion concentration relationship:

$$\Delta C = \frac{\Pi}{RT} \tag{5}$$

where R and T are the gas constant and temperature, respectively.

Detection of Alveolar Macrophage Activation and ROS Production. To probe macrophage activation, CellROX orange reagent was used (Life Technologies, Grand Island, NY, USA). Upon production of oxidative stress, CellROX reagent forms a fluorescent product whose intensity is proportional to the amount of reactive oxygen species (ROS) produced by the AM.[60] Following the same AgNP treatment and sample preparation protocols, staining was done immediately before confocal imaging. AMs were incubated in RPMI medium with 10% FBS with 5 μM CellROX reagent for 30 min in a culture incubator. After washing with PBS buffer (pH = 7.4), the samples were immediately imaged using a confocal microscope (Olympus, Flouview FV1000). The excitation and emission of CellROX orange peaked at 543 and 565 nm, respectively. Z stack images were acquired at 0.4−0.6 μm/slice, to harness intracellular fluorescent signals. We kept imaging conditions identical for all specimens to enable comparison.

Characterization of AM Cytoskeleton Integrity. Following the AgNP treatment and sample preparation protocols, AMs were fixed with 3.7% formaldehyde in PBS buffer for 30 min. After washing with PBS solution, AMs were permeabilized with 0.1% Triton-X 100 for 3 min. Upon removal of the detergent, and gentle washing with PBS, 0.17 μM Alexa568 conjugated Phalloidin (Moleclar Probes, Grand Island, NY, USA) were introduced and staining was allowed for 20 min. The dye solution was then removed by PBS washing, and the cells were imaged under confocal microscopy (Olympus, Flouview FV1000). This protocol enables detection of the actin network of the AM cytoskeleton.[61] The excitation was at 543 nm, and emission was collected 560−660 nm. Z stack images were acquired at 0.4−0.6 μm/slice, to harness intracellular fluorescent signals. We kept imaging conditions identical for all specimens to enable comparison.

Statistics. In each treatment, one control rat plus 2 rats per exposure category were used. Four to five sets of independent treatments were performed. In each in vitro cellular sample, we inspected cells under optical microscopy and determined how many representative groups there were from shape and optical contrast. For each group, we selected 3−10 cells for single-cell mechanics measurements. The overall time in each experiment was kept under 1 h to maintain fidelity of the AMs' biostatus. Single-cell mechanics measurements were carried in 33 control cells, 43 from AgNP1 exposure, 34 from AgNP2 exposure, and 24 from Ag^+ ion exposure. Post data acquisition optical analysis was performed to ensure the alignment between AFM probe and the target cell was good. The cell numbers for each treatment used for calculations after optical analysis are listed in Table 1. The quantification of force and membrane Young's modulus are shown in Table 1, as average value ± standard deviation. To compare difference in single-cell mechanics, two tailed student's t tests were performed by comparing each treatment group to the control CAMs to assess treatment impacts. Differences in means were considered significant if $p < 0.05$, and highlighted in bold font in Table 1.

■ RESULTS AND DISCUSSION

Particle Characterization. Nominal 20 and 110 nm citrate-stabilized AgNPs were utilized in this study. These AgNPs are round robin samples from the consortium by NIEHS.[49−51] The nanomaterials were manufactured using a seeded method with a 7 nm gold core and kept in 2 mM citrate buffer upon completion of reactions.[51] In addition, citrate buffer media are known to keep AgNPs well dispersed via electrostatic repulsion.[49−51] Preliminary inspection, using dynamic light scattering (DLS) and transmission electron microscopy (TEM), indicated little aggregation and determined the sizes: 19.9 ± 2.8 nm and 108.5 ± 8.8 nm, respectively.[50,51] Due to the instability of colloidal systems, AFM was utilized to verify their quality and size distribution. For AFM imaging, AgNPs were immobilized on a poly-L-lysine-coated mica (0001) surface. As shown in Figure 2, the small AgNPs (AgNP1) were well dispersed on the surface. The height of the two representative AgNP1 particles were 21.9 nm (particle on left) and 21.1 nm (particle on right), as indicated by the red line drawn through the two particles and red cursor profile below (Figure 2A). The mean diameter of 53 AgNP1 particles was measured and found to be 20 ± 2 nm, which was in good agreement with the results of initial DLS and TEM measurements. The larger AgNPs (AgNP2) were also well dispersed on the mica surface (Figure 2B), and the mean diameter was measured as 96 ± 9 nm, which was consistent with manufacturer measurements. The AFM images indicate that both AgNPs were well dispersed before intratracheal instillation.

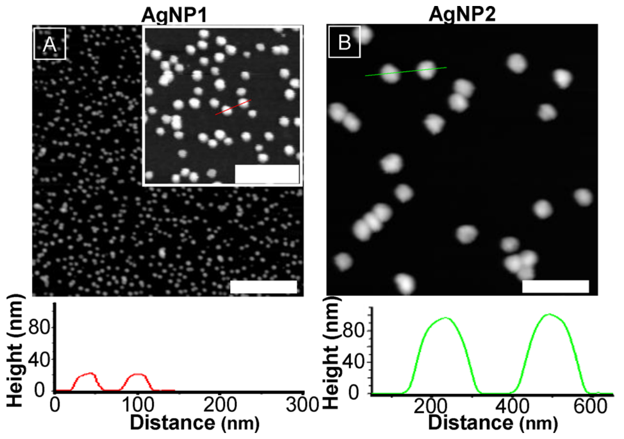

Figure 2. AFM topography images of (A) AgNP1 and (B) AgNP2 immobilized onto poly-L-lysine coated mica (0001) surfaces. AFM images were acquired under ambient conditions using a silicon cantilever. Scale bar = 500 nm. Inset: 2(A) shows a zoom-in view to reveal AgNP2 more clearly. Scale bar = 200 nm for the inset. Cursor profiles are indicated in and shown below the corresponding images.

Single-Cell Mechanics of Primary Alveolar Macrophages upon Instillation of 20 nm AgNPs. Previous study indicates that citrate buffer has little acute impact on lung inflammatory responses.[54] Therefore, 2 mM citrate buffer instillation, abbreviated as CAM treatment, was used as control for this investigation. The citrate buffer treatment allows accurate extraction of the effect by AgNPs on the macrophage, as the buffers serve as media for AgNPs to disperse within. A typical force vs ε profile for AM-CAM, AM recovered from rats after IT of citrate buffer, is shown in Figure 3 (black curve). The cell measured was 13.2 μm tall and its force profile appeared smooth and nonlinear. The morphology and mechanics are almost identical to that recovered from rat lungs without any treatment; therefore, our technology confirms that CAM provides a good reference and control for this investigation. The mechanical strength of the AM-CAM fell between that of a mouse neuroblastoma (N2a) cell and a human Jurkat T cell.[41,45] It requires 28.9 and 144 nN to compress the cell by 30% and 60% of its original height, respectively. To achieve the same degree of compression (30% and 60%), N2a cells require 6.6 and 63 nN, and Jurkat T cells require 23 and 163 nN, respectively.[41,45] The membrane Young's modulus (E_m) of the control AM-CAM extracted from the nonlinear fitting to its force profile is 1.4 MPa. The same fitting also yielded cytoskeleton modulus E_c = 3.0 kPa. All AMs-

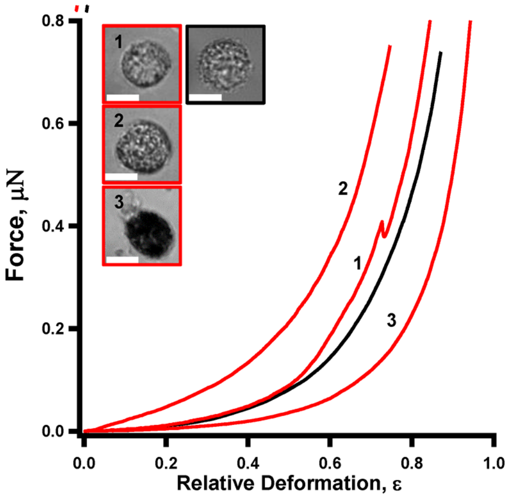

Figure 3. Typical F vs ε profiles for primary AMs upon exposure to citrate buffer (control, black) and AgNP1 (red lines). Three distinct mechanical behaviors were observed in comparison to the control cells: unchanged (curve 1), stiffer (curve 2), and softer (curve 3). Insets show optical images of the corresponding AM cells prior to compression. Scale bar = 10 μm.

CAM appeared round and with relative homogeneous intracellular optical contrast, as shown in Figure 3 (inset, black frame). The morphology and mechanical property among all control experiments are summarized in Table 1, where the cell height measured 12.9 ± 1.3 μm, $E_m = 1.1 \pm 0.5$ MPa, and $E_c = 5.9 \pm 2.7$ kPa. Overall, the control cells exhibit a high degree of homogeneity and consistency in both morphology and force profile.

Upon in vivo exposure to AgNP1 (referred to as AgNP1-CAM treatment), we observed a high degree of variation among cells harvested, under optical microscopy as well as single-cell mechanics measurements. These observations intrinsically differ from our prior investigation of nanocytotoxicity upon in vitro treatments.[46] Human aortic endothelial cells (HAECs) reveal relatively homogeneous responses upon ZnO NP treatment, with the majority of populations exhibiting increases in membrane elastic compliance at the dosage of 10 μg/mL.[46] Therefore, the single-cell-based approach is more critical in this investigation to probe the genuine outcome of the cellular responses to NPs. Three types of mechanical profiles are representative among AMs upon AgNP1-CAM: (1) unchanged, (2) stiffer than control, as indicated by the left-shift of force vs ε profile, and (3) softer, as indicated by the right-shift of force profile. The cellular populations are 42%, 16%, and 42%, respectively. Figure 3 reveals the three profiles from representative cells. For stiffened AMs (e.g., red curve 2), it requires 84 and 341 nN force to deform the cell by 30% and 60%, respectively. This is nearly twice as much force as that for controls (black curve). $E_m = 1.5$ MPa, which is similar to that of AM-CAM, whereas E_c increases to 14.1 kPa, indicating a stiffer cytoskeleton. Among all stiffened cells, $E_m = 1.1 \pm 0.6$ MPa and $E_c = 12.5 \pm 6.9$ kPa (see also Table 1). The observed stiffening is consistent with the rearrangement of the macrophage cytoskeleton, as prior investigations indicated that endocytosis or phagocytosis of AMs could lead to actin rearrangement.[62−64] For AM cells from AgNP1-CAM treatment with softer profiles (e.g., Figure 3, red curve 3), Young's moduli measure $E_m = 0.5$ MPa and $E_c = 1.4$ kPa. Among all softened cells measured, the $E_m = 0.3 \pm 0.2$ MPa, significantly smaller than that in controls. In addition, the E_c also decreases to 2.2 ± 1.2 kPa, about one-third that of the controls (5.9 ± 2.7 kPa). The cells do not seem to swell or alter the morphology, e.g., height = 12.9 ± 1.3 μm, which is very similar to that of the AMs-CAM. Therefore, we infer that AgNP1 uptake and its intracellular accumulation damages the cellular membrane and disrupts the cytoskeleton network, which is analogous to the previously known damages by AgNPs to other cell types such as fibroblast cells and cortical neurons.[7,65,66]

To check the AgNP1 intake in all three responses, we examined the corresponding optical images (see examples shown in Figure 3, insets) and quantified the darkness scores. The dark contrast, i.e., less transmission of photons, is due to intracellular nanoparticles (typically aggregates), as reported previously.[7,12,19] For cells shown in Figure 3, the darkness scores are 1.1 for control and 5.6, 15.4, and 61.2 for curves 1, 2, and 3, respectively. Among all the control cells (AMs-CAM) examined, the darkness score range is 0.2−3.5, which serves as a reference to evaluate AgNP intake. With 2X and 6X of the control darkness as threshold, i.e., score = 7 and 21, cells represented by curve 2 mostly fall into medium (7−21) AgNP1 intake, whereas cells represented by curve 3 are high (21−62) darkness. For AMs from AgNP1-CAM treatment that are harder than AMs-CAM, we observe a darkness score range of 1.3−15.4, i.e., mostly medium darkness score. The softer cells indicate a high amount of intracellular AgNPs. These observations further support our previous conclusions deduced from single-cell mechanics measurements, where higher uptake led to disruption of cytoskeleton. In addition, the single-cell mechanics is evidently more sensitive and potentially more quantitative to cellular changes than optical inspection (compare responses 1 and 2).

To verify cellular damages suggested by cellular mechanics measurements and probe the activation status of AMs, reactive oxygen species (ROS) production and F-actin network were investigated. Using identical conditions as AgNP1 treatments discussed above, we stained the AMs upon harvesting to CellROX reagent to probe ROS production.[60] CellROX emission is at 565 nm, the intensity reflecting the ROS produced by the macrophages at the designed time. Figure 4 compares the results from control CAM cells (Figure 4A) with those post AgNP1 exposures (Figure 4B−D). All CAM cells exhibited a very low fluorescence signal, indicating low ROS production and lack of activation among AMs. All AMs from AgNP1-CAM treatment showed elevated ROS production in comparison to controls. Panels B−D of Figure 4 show the three representative confocal images corresponding to low, medium, and high AgNP1 uptake, with darkness scores of 4.4, 12.2, and 25.3, respectively. At low to medium AgNP1 intake (Figure 4B,C), the ROS intensity is higher than that under high intracellular AgNP1 (Figure 4D). This is consistent with the time profile of the ROS-based cytotoxic effect, where the ROS production increases and peaks during initial AgNP uptake and then decreases upon cytoskeleton damage, and decreased viability and NADPH oxidase activities.[67−70]

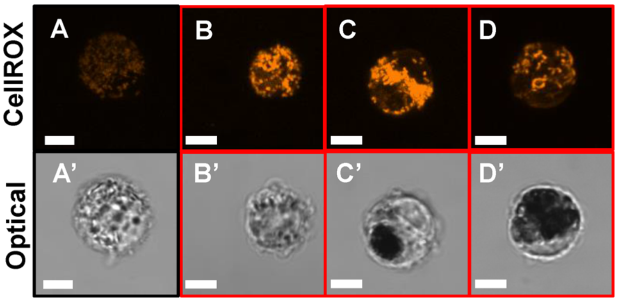

Figure 4. Z-stacking confocal images of AMs from control CAM treatment (A), and AgNP1-CAMs treatment (B−D) stained with CellROX (orange) to reveal intracellular ROS production. The intensity of orange contrast reflects the amount of ROS produced by the macrophage. The corresponding bright field optical images are displayed below to reveal the amount of intracellular AgNP 1s. Scale bar = 5 μm.

Figure 5 illustrates the changes of AM F-actin network due to IT of AgNP1. The control cell (Figure 5A) has well-defined stress fibers and dense, actin-rich lamella podia. This observation is consistent with the conclusion that citrate buffer (2 mM) had little impact on AMs. Panels B−D of Figure 5 reveal the intracellular distributions and integrity of F-actin that correspond to low, medium, and high intracellular AgNP1, with darkness scores of 1.7 (Figure 5B), 1.3 (Figure 5D1), 6.2 (Figure 5C), and 25.9 (Figure 5D2), respectively. The amount of intracellular AgNP1 correlates well with the increasing degradation of actin network among AMs from AgNP1-CAM

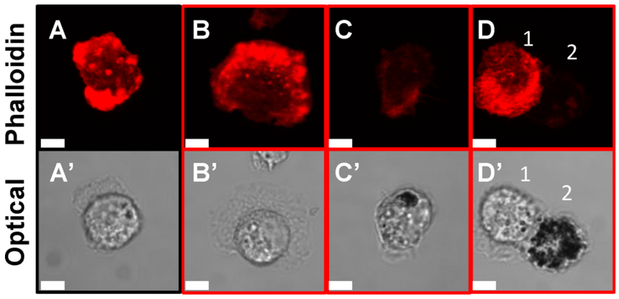

Figure 5. Z-stacking confocal images of AMs with treatment of CAM (A) and AgNP1-CAMs (B-D). All cells are stained with Alexa Fluor 568 conjugated phalloidin to reveal the changes of cytoskeleton F-actin. The corresponding bright field optical images are displayed below to reveal the intracellular AgNP1 uptake. Scale bar = 5 μm.

treatment. The AM from AgNP1-CAM treatment with high intracellular AgNPs (Figure 5D′2) exhibit very low fluorescence intensity, indicating severe damage of the cytoskeletal actin network.

Longer post time exposure reveals that the population of stiffening and damaged cells decreases significantly after 7 days, and only a small portion is detectable after 21 days. This observation further demonstrates that mechanical changes were caused by AgNP exposure and took a long time to clear and recover. Because the current study focuses on the acute effects of AgNPs on AM cells, we keep our focus on the AMs collected 24 h post exposure.

Single-Cell Mechanics of Primary Alveolar Macrophages upon Instillation of 110 nm AgNPs. Upon instillation of 0.5 mg/kg b.w. of AgNP2 (110 nm), we found three types of mechanical behaviors among the AMs that are similar to those of AgNP1 exposure: (1) unchanged, (2) stiffer than control, and (3) softer than control. Figure 6 reveals the three mechanical profiles from representative cells. The cellular populations are 39%, 17%, and 44% among the three mechanical responses. The examples of all three responses are shown in Figure 6.

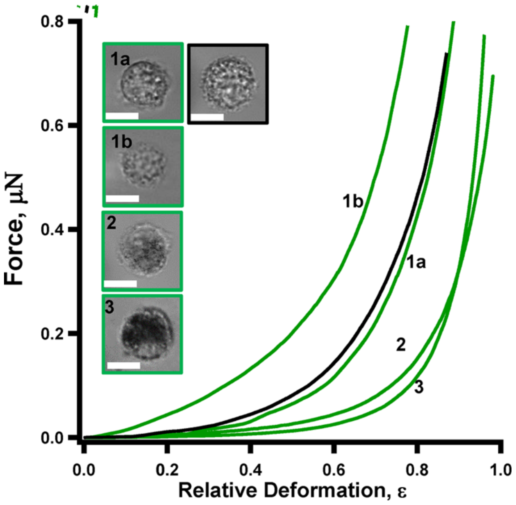

Figure 6. Typical F vs ε profiles for primary AMs upon exposure to citrate buffer (control, black), and AgNP2 by IT (green lines). Three distinct mechanical behaviors were observed in comparison to the control cells: unchanged (curve 1a), stiffer (curve 1b), and softer (2 and 3). Insets show optical images of the corresponding AMs prior to compression. Scale bar = 10 μm.

Although the cellular mechanics are similar to that of AgNP1 exposures, the corresponding AgNP2 intake reveals some subtle differences. Following similar procedures as that in comparing 20 nm AgNP intake, the darkness score for AMs-AgNP2-CAMs were measured. Insets 1a and 1b in Figure 6 belong to low uptake (score = 2.6 and 1.8, respectively), inset 2 is medium darkness (score = 11.6), and inset 3 represents a high uptake (score = 31.2). Unlike AgNP1, we did not observe a darkness score higher than 56, among all AMs from AgNP2-CAM experiments. This is an indication that 110 nm Ag NPs exhibit less intracellular aggregation than 20 nm AgNPs under the same exposure conditions.

For AMs with a mechanical profile (Figure 6, green curve 1a) similar to that of AMs from CAM treatment (black curve), their cellular morphology such as height, shape, and spreading appeared to be very similar to that of controls (Figure 6, insets). For AM cells harder than controls (e.g., green curve 1b), it requires a higher load, 81 and 305 nN, to reach 30% and 60% deformation, respectively. The forces are nearly twice as much as that for controls (black curve). The nonlinear fitting of the force profile yields E_m = 0.9 MPa and E_c = 19.6 kPa. The morphologies among cells with stiffer profiles were very similar to those of the control, with height 14.8 ± 1.1 μm. Analogous to AgNP1 treatment, the stiffening of AMs is likely due to the rearrangement of cytoskeleton caused by activated phagocytosis.[64] For AgNP2-CAM treated cells exhibiting softer mechanics, two examples were shown in Figure 6 (green curves 2 and 3), representing low and medium AgNP intake. At low intake, the E_m = 0.2 MPa and E_c = 0.5 kPa. At higher AgNP intake E_m = 0.2 MPa and E_c = 2.1 kPa, which are similar to values for low intake. Among cells with softened mechanics, E_m = 0.3 ± 0.2 MPa and E_c = 1.1 ± 0.6 kPa, significantly softer than values for the control (p-value <0.05). These observations indicate that AgNP2 also damages the cell membrane and disrupts the actin cytoskeleton network.

To verify cellular damages suggested by cell mechanics measurements and probe the activation status of AMs, ROS production and F-actin network were investigated following the same protocols used in AgNP1 exposure. Figure 7 compares the results of AMs from control CAM treatment with those for AgNP2 exposure. All AMs from AgNP2-CAM treatment showed elevated ROS production in comparison to the cases

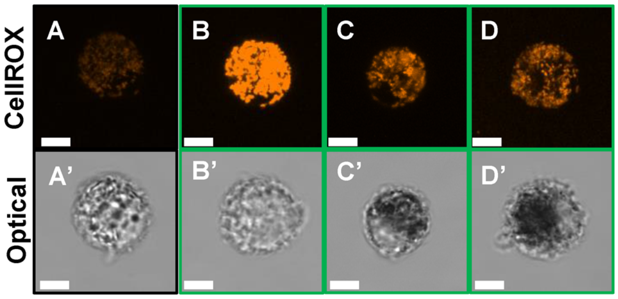

Figure 7. Z-stacking confocal images of AMs from control CAM treatment (A) and AgNP2-CAM treatment (B−D) staining with CellROX (orange) to reveal intracellular ROS production. The intensity of orange contrast reflects the amount of ROS produced by the macrophage. The corresponding bright field optical images are displayed below to reveal the amount of intracellular AgNP 2s. Scale bar = 5 μm.

of the controls, regardless of the amount of intracellular AgNP2 aggregates. Panels B−D of Figure 7 show the three representative confocal images corresponding to low, medium, and high AgNP2 uptake, with darkness scores of 2.8, 15.0, and 23.4, respectively. At low to medium AgNP2 intake (Figure 7B,C), the ROS intensity is higher than that under high intracellular AgNP2 (Figure 7D). This is very similar to the trend observed in the case of AgNP1 exposure.

Figure 8 illustrates the changes of the AM F-actin network due to AgNP2 instillation. Compared with the image of the control cell (Figure 8A) that has well-defined stress fibers and dense, actin-rich lamella podia, panels B−D of Figure 8 reveal the intracellular distributions and integrity of F-actin, which correspond to low, medium, and high intracellular AgNP2, with darkness scores of 2.0, 8.0, and 21.8, respectively. The amount of intracellular AgNP2 correlates well with the increasing degradation of actin network among AMs-AgNP2-CAM. Clearly, AgNP2-CAM with high intracellular AgNP 2s (Figure 8D′) exhibits low fluorescence intensity, indicating severe damage of the cytoskeletal actin network. However, the impacts of AgNP2 on F-actin disruption are less pronounced compared to that of AgNP1. Even with moderate intracellular AgNP2 intake, AM-AgNP2-CAM still exhibit a well preserved actin cytoskeleton (Figure 8C). It requires high intracellular AgNP2 intake to reach comparable degradation of F-actin caused by moderate AgNP1 intake, comparing Figure 8D with Figure 5C.

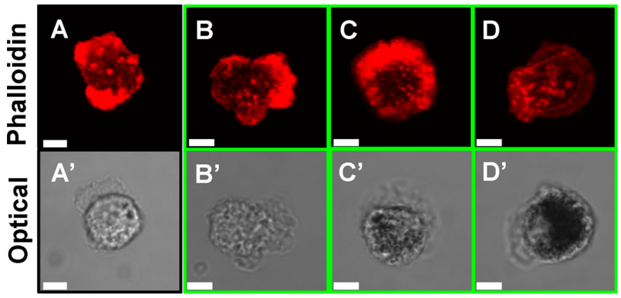

Figure 8. Z-stacking confocal images of AM-CAM (A) and AMs-AgNP2-CAM (B−D) staining with Alexa fluor 568 conjugated phalloidin to highlight the changes of cytoskeleton F-actin. The corresponding bright field optical images are displayed below to reveal the intracellular AgNP2 aggregates. Scale bar = 5 μm.

Taken collectively, these results demonstrate that single-cell-based technology is necessary because of the variations in AgNP intake and responses among cells in the situations of in vivo exposures. In both treatments, the mechanics measurements clearly reveal that about 20% of AMs take up very little AgNPs, whereas about 40% population has moderate or high intake of nanoparticles. In addition, single-cell mechanics provides an informative readout of the AgNP−cell interactions. Both AgNPs exhibit similar trends with the increasing intracellular AgNPs: low intake of NPs leads to stiffening of the cells due to rearrangement of cytoskeleton, whereas higher intracellular AgNPs manifest softening of the cells due to higher ROS production and cytoskeleton damages. This trend is confirmed by the measurements of ROS production and actin-network imaging. Our investigations also reveal some differences between 20 and 110 nm AgNPs under the same dosage and exposure time. The 110 nm AgNPs exhibit less damage of the actin-network (compare Figures 5 and 8) than of 20 nm AgNP treatments. These findings are in agreement with other studies which also found that bigger AgNPs are less toxic than smaller ones.[11,20,51] Our results further indicate that 20 nm AgNPs enter AM cells more readily than larger ones, and aggregations often occur leading to higher darkness scores. In the case of 110 nm AgNP exposures, single-cell mechanics senses the stiffening even when the amount of intracellular AgNPs is not detectable from optical imaging. The force-deformation profiles could probe quantitatively the structural and mechanical changes of membrane and cytoskeleton.[41,42,44−46,58] The mechanism of different responses among AMs to AgNPs in vivo is not yet clear to us, due partly to the complexity and variation in microenvironment of the lung.[11,13,19−21,65] This aspect warrants further technology development and in vivo investigations in situ.

Single-Cell Mechanics of AMs upon Instillation of Solutions Containing Ag(I). To verify that the damage of AgNPs is due to nanoparticles instead of Ag(I) ions, we measured AM mechanics after IT of solutions containing Ag^+. Soluble Ag(I) or Ag^+ in the form of silver nitrate solution was instilled directly into the rat lung at a concentration of 0.05 mg Ag^+/kg body weight. The concentration of Ag^+ was chosen on the basis of the knowledge that ∼5−6% of AgNPs dissolved in culture medium and intracellularly within 24 hours.[14,51,66,71] A typical force vs ε profile for AMs post IT of Ag^+ (abbreviated as AM-Ag^+(0.05)) is shown in Figure 9. In comparison to the AgNP exposures, Ag ion treatments exhibit one similarity and three significant differences. Similar to nanoparticle treatments, the AM-Ag^+(0.05) cell is harder than control. It requires 53 and 258 nN of force to reach 30% and 60% deformation for the AM-Ag^+(0.05), respectively, which are higher than those of controls. Unlike AgNP treatments, the AMs-Ag^+(0.05) show less heterogeneity: height = 16.8 ± 0.5 μm, E_m = 0.9 ± 0.6 MPa, and E_c = 7.2 ± 1.6 kPa. Under optical microscopy, cells appear round and have almost identical darkness scores (0.1−2.6) as control (0.2−3.5), as also summarized in Table 1. In addition, the silver ions caused cellular swelling, e.g., height = 16.7 μm with a cell volume of 5200 μm^3. Finally, there is little

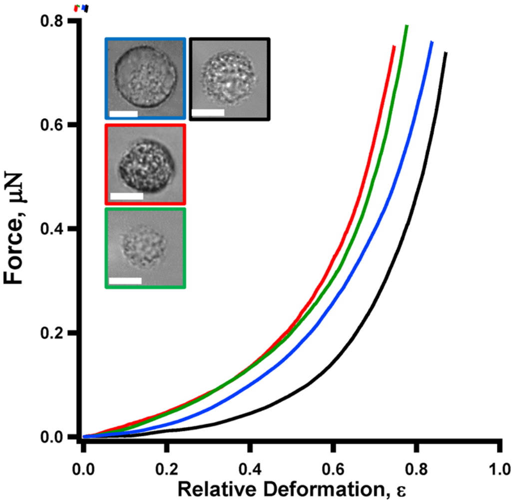

Figure 9. Typical F vs ε profiles for a AM-CAM (control, black), an AM after IT with 0.05 mg Ag^+/kg b.w. (blue), a AM-AgNP1-CAM (red), and a AM-AgNP2-CAM (green). AM cells are selected from populations exhibiting stiffer responses than the control, to be compared with Ag^+ treatments and elucidating mechanism. Scale bar = 10 μm.

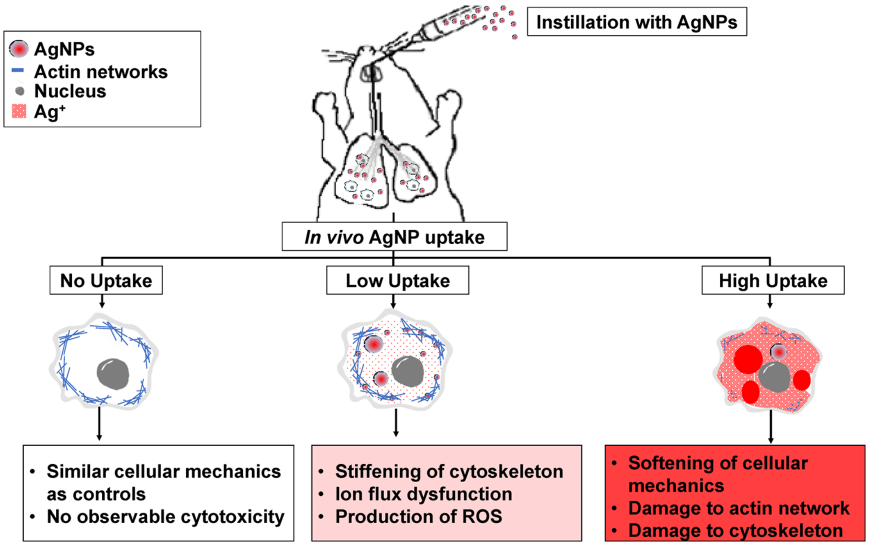

Figure 10. Schematic diagram illustrating interactions between AgNPs and AMs and the resulting cellular responses upon instillation of AgNPs.

softening observed for AMs-Ag^+(0.05). In other words, Ag ions led to little damage of membrane or cytoskeleton.

Because the cellular volume of AM-Ag^+(0.05) was approximately twice that of the control AM-CAM (Table 1), ion-flux dysfunction was likely taking place leading to swelling. This is also consistent with a prior report that Ag^+ could interact with membrane and proteins leading to dysfunction of ion channels.[72] Following previously established procedures (also briefly described in Experimental Methods),[45,46] one could quantify the ion flux dysfunction. The change in intracellular ion concentration (ΔC), extracted from the force profiles, is 18.7 ± 12.2 μM for AMs-Ag^+(0.05). If applying the ion flux dysfunction model forcefully to AgNP treated AMs, the ΔC values are 34.8 ± 13.3 and 56.1 ± 15.6 μM for AMs-AgNP1-CAM and AMs-AgNP2-CAM, respectively. Both values are higher than those for Ag ion treatment, which are not valid chemically or physically, as the ion concentration is not nearly as high as AMs-Ag^+(0.05), and AgNPs do not lead to swelling of cells. Therefore, we conclude that the ion flux dysfunction model is not valid in the case of AgNP treatments, nor the key cause of the stiffening among these stiffened cells. In other words, the changing of cytoskeleton structures is primarily responsible for the stiffening of AMs cells. Because Ag^+ did not cause softening of cells, we infer that the AgNPs are solely responsible for formation of ROS and ROS based damages. Prior reports indicated that ambient oxygen could react with AgNPs, forming peroxide intermediates, such as hydroxyl radicals, superoxide, hydrogen peroxide, and single oxygen.[9,73] Given the acidic environment inside the AM cell, these reactions are likely the chemical basis for generation of ROS, which led to the damage of cellular membrane and cytoskeleton. The relatively high uncertainty is another indication of the heterogeneity among AMs upon NP exposure in vivo. Therefore, we note that single-cell-based approaches should be utilized to probe these interactions.

■ CONCLUSIONS

Using a simple in vitro method of single-cell mechanics, this work demonstrates that single-cell-based measurements are important and necessary to reveal interactions between AgNPs and AM cells upon in vivo exposure, such as intratracheal instillation. Single-cell mechanics reveals three primary scenarios as summarized in Figure 10: (1) little to no intake of AgNPs, which leads to no mechanical changes in comparison to the case of the control; (2) low to medium uptake of AgNPs, which results in rearrangement of cytoskeleton, which is primarily responsible for cellular stiffening; (3) high amount of intracellular AgNPs, which elicits ROS production and AM actions, eventually leading to disintegration of actin network in the cytoskeleton, manifesting in softening of cellular mechanics. The conclusions regarding interactions and responses were verified by optical microscopy in situ, whose darkness score allows comparison of the AgNP uptakes, as well as by single-cell-based fluorescence microscopy to image ROS production and cytoskeleton integrity. The results from this investigation offer important insights into the NP−cell interactions in vivo and reveal the complexity and heterogeneity of the cellular responses. This information shall hopefully attract further technology development, such as in situ functional tests, to study nanoparticle−cell interactions in vivo. Given the single-cell nature of this method, work is in progress to give this approach higher throughput in the future.

■ AUTHOR INFORMATION

Corresponding Author

*G.-y. Liu. E-mail: gyliu@ucdavis.edu. Phone: 530-754-96678. Fax: 530-754-8557.

Notes

The authors declare no competing financial interest.

■ ACKNOWLEDGMENTS

We thank Dr. C. C. Fleming for helpful discussions, Ms. S. Stagner and Dr. S. Smiley-Jewell for their assistance in the preparation of this manuscript. We are grateful to Ryan Mendoza, Imelda Espiritu, and Janice Peake at UCD Center for Health & the Environment (CHE) for their technical assistance during handling of animals. Reviewer 1's critiques and comments improved the quality and clarity of this paper. This work was supported by the W. M. Keck Foundation, University of California Davis. Grant support (U01 ES020127) and silver nanomaterials used in this study are procured, characterized, and provided by NIEHS Centers for Nanotechnology Health Implications Research (NCNHIR) Consortium. D.S.A. is a recipient of a Superfund Research Program Fellowship (P42 ES004699). Y.X.L is a recipient of the GAANN Fellowship from the United States Department of Education (2009-2010). R.M.S. is a recipient of a Western Center for Agricultural Health and Safety Fellowship (NIOSH Grant 0H07550). The content is solely the responsibility of the authors and does not represent the official views of the National Institutes of Health. The NIEHS Centers for Nanotechnology Health Implications Research (NCNHIR) was established with the centers funded by RFA-ES-09-011. These centers formed a consortium with other NIEHS funded researchers in the area of Nano EHS and worked together on a select set of engineered nanomaterials provided to the consortium by NIEHS. Any opinions, findings, conclusions, or recommendations expressed herein are those of the author(s) and do not necessarily reflect the views of the National Institute of Environmental Health Sciences or NIH.

■ ABBREVIATIONS

IT: intratracheal instillation
NP: nanoparticle
BAL: bronchoalveolar lavage
BALF: bronchoalveolar lavage fluid
AFM: atomic force microscopy
SD: Sprague−Dawley
AM: alveolar macrophage
CAM: treatment with citrate buffer
AMs-CAM: alveolar macrophages recovered from rats after IT with citrate buffer
AgNP1-CAM: treatment with AgNP1 in citrate buffer
AMs-AgNP1-CAM: alveolar macrophages recovered from IT with AgNP1 in citrate buffer
AgNP2-CAM: treatment with AgNP2 in citrate buffer
AMs-AgNP2-CAM: alveolar macrophages recovered from IT with AgNP2 in citrate buffer
Ag^+(0.05): treatment with 0.05 mg of Ag^+/kg of body weight
AMs-Ag^+(0.05): alveolar macrophages recovered from IT with Ag^+
ROS: reactive oxygen species

■ REFERENCES

(1) Ahamed, M.; Alsalhi, M. S.; Siddiqui, M. K. Silver Nanoparticle Applications and Human Health. *Clin. Chim. Acta* **2010**, *411*, 1841−1848.

(2) Tran, Q. H.; Nguyen, V. Q.; Le, A.-T. Silver Nanoparticles: Synthesis, Properties, Toxicology, Applications and Perspectives. *Adv. Nat. Sci.: Nanosci. Nanotechnol.* **2013**, *4*, 033001.

(3) Pelgrift, R. Y.; Friedman, A. J. Nanotechnology as a Therapeutic Tool to Combat Microbial Resistance. *Adv. Drug Delivery Rev.* **2013**, *65*, 1803−1815.

(4) Lee, J. H.; Ahn, K.; Kim, S. M.; Jeon, K. S.; Lee, J. S.; Yu, I. J. Continuous 3-Day Exposure Assessment of Workplace Manufacturing Silver Nanoparticles. *J. Nanopart. Res.* **2012**, *14*, 1−10.

(5) Nowack, B.; Ranville, J. F.; Diamond, S.; Gallego-Urrea, J. A.; Metcalfe, C.; Rose, J.; Horne, N.; Koelmans, A. A.; Klaine, S. J. Potential Scenarios for Nanomaterial Release and Subsequent Alteration in the Environment. *Environ. Toxicol. Chem.* **2012**, *31*, 50−59.

(6) Quadros, M. E.; Marr, L. C. Environmental and Human Health Risks of Aerosolized Silver Nanoparticles. *J. Air Waste Manage. Assoc.* **2010**, *60*, 770−781.

(7) Liu, H.; Yang, D.; Yang, H.; Zhang, H.; Zhang, W.; Fang, Y.; Lin, Z.; Tian, L.; Lin, B.; Yan, J.; et al. Comparative Study of Respiratory Tract Immune Toxicity Induced by Three Sterilisation Nanoparticles: Silver, Zinc Oxide and Titanium Dioxide. *J. Hazard. Mater.* **2013**, *248−249*, 478−486.

(8) Geiser, M. Update on Macrophage Clearance of Inhaled Micro- and Nanoparticles. *J. Aerosol Med. Pulm. Drug Delivery* **2010**, *23*, 207−217.

(9) Liu, J.; Hurt, R. H. Ion Release Kinetics and Particle Persistence in Aqueous Nano-Silver Colloids. *Environ. Sci. Technol.* **2010**, *44*, 2169−2175.

(10) Stensberg, M. C.; Wei, Q.; McLamore, E. S.; Porterfield, D. M.; Wei, A.; Sepulveda, M. S. Toxicological Studies on Silver Nanoparticles: Challenges and Opportunities in Assessment, Monitoring and Imaging. *Nanomedicine (London, U. K.)* **2011**, *6*, 879−898.

(11) Hamilton, R. F.; Buckingham, S.; Holian, A. The Effect of Size on Ag Nanosphere Toxicity in Macrophage Cell Models and Lung Epithelial Cell Lines is Dependent on Particle Dissolution. *Int. J. Mol. Sci.* **2014**, *15*, 6815−6830.

(12) Wang, H.; Wu, L.; Reinhard, B. M. Scavenger Receptor Mediated Endocytosis of Silver Nanoparticles into J774a.1 Macrophages is Heterogeneous. *ACS Nano* **2012**, *6*, 7122−7132.

(13) Singh, R. P.; Ramarao, P. Cellular Uptake, Intracellular Trafficking and Cytotoxicity of Silver Nanoparticles. *Toxicol. Lett.* **2012**, *213*, 249−259.

(14) Haase, A.; Tentschert, J.; Jungnickel, H.; Graf, P.; Mantion, A.; Draude, F.; Plendl, J.; Goetz, M. E.; Galla, S.; Masic, A.; et al. Toxicity of Silver Nanoparticles in Human Macrophages: Uptake, Intracellular Distribution and Cellular Responses. *J. Phys.: Conf. Ser.* **2011**, *304*, 012030.

(15) Thompson, E. A.; Sayers, B. C.; Glista-Baker, E. E.; Shipkowski, K. A.; Taylor, A. J.; Bonner, J. C. Innate Immune Responses to Nanoparticle Exposure in the Lung. *J. Environ. Immunol. and Toxicol.* **2014**, *1*, 150−156.

(16) Kim, S.; Choi, I. H. Phagocytosis and Endocytosis of Silver Nanoparticles Induce Interleukin-8 Production in Human Macrophages. *Yonsei Med. J.* **2012**, *53*, 654−657.

(17) Gordon, S. B.; Read, R. C. Macrophage Defences against Respiratory Tract Infections. *Br. Med. Bull.* **2002**, *61*, 45−61.

(18) Sung, J. H.; Ji, J. H.; Yoon, J. U.; Kim, D. S.; Song, M. Y.; Jeong, J.; Han, B. S.; Han, J. H.; Chung, Y. H.; Kim, J.; et al. Lung Function Changes in Sprague-Dawley Rats after Prolonged Inhalation Exposure to Silver Nanoparticles. *Inhalation Toxicol.* **2008**, *20*, 567−574.

(19) Carlson, C.; Hussain, S. M.; Schrand, A. M.; Braydich-Stolle, L. K.; Hess, K. L.; Jones, R. L.; Schlager, J. J. Unique Cellular Interaction of Silver Nanoparticles: Size-Dependent Generation of Reactive Oxygen Species. *J. Phys. Chem. B* **2008**, *112*, 13608−13619.

(20) Park, M. V. D. Z.; Neigh, A. M.; Vermeulen, J. P.; de la Fonteyne, L. J. J.; Verharen, H. W.; Briede, J. J.; van Loveren, H.; de Jong, W. H. The Effect of Particle Size on the Cytotoxicity, Inflammation, Developmental Toxicity and Genotoxicity of Silver Nanoparticles. *Biomaterials* **2011**, *32*, 9810−9817.

(21) Park, E. J.; Yi, J.; Kim, Y.; Choi, K.; Park, K. Silver Nanoparticles Induce Cytotoxicity by a Trojan-Horse Type Mechanism. *Toxicol. In Vitro* **2010**, *24*, 872−878.

(22) Kroll, A.; Pillukat, M. H.; Hahn, D.; Schnekenburger, J. Current in Vitro Methods in Nanoparticle Risk Assessment: Limitations and Challenges. *Eur. J. Pharm. Biopharm.* **2009**, *72*, 370−377.

(23) Sayes, C. M.; Reed, K. L.; Warheit, D. B. Assessing Toxicity of Fine and Nanoparticles: Comparing in Vitro Measurements to in Vivo Pulmonary Toxicity Profiles. *Toxicol. Sci.* **2007**, *97*, 163−180.

(24) Alger, H.; Momcilovic, D.; Carlander, D.; Duncan, T. V. Methods to Evaluate Uptake of Engineered Nanomaterials by the Alimentary Tract. *Compr. Rev. Food Sci. Food Saf.* **2014**, *13*, 705−729.

(25) Ruge, C. A.; Schaefer, U. F.; Herrmann, J.; Kirch, J.; Canadas, O.; Echaide, M.; Perez-Gil, J.; Casals, C.; Muller, R.; Lehr, C. M. The Interplay of Lung Surfactant Proteins and Lipids Assimilates the Macrophage Clearance of Nanoparticles. *PLoS One* **2012**, *7*, e40775.

(26) Han, X.; Corson, N.; Wade-Mercer, P.; Gelein, R.; Jiang, J.; Sahu, M.; Biswas, P.; Finkelstein, J. N.; Elder, A.; Oberdorster, G. Assessing the Relevance of in Vitro Studies in Nanotoxicology by

Examining Correlations between in Vitro and in Vivo Data. *Toxicology* **2012**, *297*, 1−9.

(27) Rushton, E. K.; Jiang, J.; Leonard, S. S.; Eberly, S.; Castranova, V.; Biswas, P.; Elder, A.; Han, X.; Gelein, R.; Finkelstein, J.; et al. Concept of Assessing Nanoparticle Hazards Considering Nanoparticle Dosemetric and Chemical/Biological Response Metrics. *J. Toxicol. Environ. Health, Part A* **2010**, *73*, 445−461.

(28) Love, S. A.; Maurer-Jones, M. A.; Thompson, J. W.; Lin, Y. S.; Haynes, C. L. Assessing Nanoparticle Toxicity. *Annu. Rev. Anal. Chem.* **2012**, *5*, 181−205.

(29) Ong, K. J.; MacCormack, T. J.; Clark, R. J.; Ede, J. D.; Ortega, V. A.; Felix, L. C.; Dang, M. K.; Ma, G.; Fenniri, H.; Veinot, J. G.; et al. Widespread Nanoparticle-Assay Interference: Implications for Nanotoxicity Testing. *PLoS One* **2014**, *9*, e90650.

(30) Gavara, N.; Chadwick, R. S. Determination of the Elastic Moduli of Thin Samples and Adherent Cells Using Conical Atomic Force Microscope Tips. *Nat. Nanotechnol.* **2012**, *7*, 733−736.

(31) Dufrene, Y. F.; Pelling, A. E. Force Nanoscopy of Cell Mechanics and Cell Adhesion. *Nanoscale* **2013**, *5*, 4094−4104.

(32) Plodinec, M.; Loparic, M.; Monnier, C. A.; Obermann, E. C.; Zanetti-Dallenbach, R.; Oertle, P.; Hyotyla, J. T.; Aebi, U.; Bentires-Alj, M.; Lim, R. Y.; et al. The Nanomechanical Signature of Breast Cancer. *Nat. Nanotechnol.* **2012**, *7*, 757−765.

(33) Rico, F.; Roca-Cusachs, P.; Gavara, N.; Farre, R.; Rotger, M.; Navajas, D. Probing Mechanical Properties of Living Cells by Atomic Force Microscopy with Blunted Pyramidal Cantilever Tips. *Phys. Rev. E Stat. Nonlin. Soft Matter. Phys.* **2005**, 72, 021914.

(34) Iyer, S.; Gaikwad, R. M.; Subba-Rao, V.; Woodworth, C. D.; Sokolov, I. Atomic Force Microscopy Detects Differences in the Surface Brush of Normal and Cancerous Cells. *Nat. Nanotechnol.* **2009**, *4*, 389−393.

(35) Haase, K.; Pelling, A. E. Investigating Cell Mechanics with Atomic Force Microscopy. *J. R. Soc., Interface* **2015**, *12*, 20140970.

(36) Li, Q. S.; Lee, G. Y.; Ong, C. N.; Lim, C. T. Afm Indentation Study of Breast Cancer Cells. *Biochem. Biophys. Res. Commun.* **2008**, *374*, 609−613.

(37) Bongiorno, T.; Kazlow, J.; Mezencev, R.; Griffiths, S.; Olivares-Navarrete, R.; McDonald, J. F.; Schwartz, Z.; Boyan, B. D.; McDevitt, T. C.; Sulchek, T. Mechanical Stiffness as an Improved Single-Cell Indicator of Osteoblastic Human Mesenchymal Stem Cell Differentiation. *J. Biomech.* **2014**, *47*, 2197−2204.

(38) Nawaz, S.; Sanchez, P.; Bodensiek, K.; Li, S.; Simons, M.; Schaap, I. A. Cell Visco-Elasticity Measured with Afm and Optical Trapping at Sub-Micrometer Deformations. *PLoS One* **2012**, *7*, e45297.

(39) Lal, R.; Ramachandran, S.; Arnsdorf, M. F. Multidimensional Atomic Force Microscopy: A Versatile Novel Technology for Nanopharmacology Research. *AAPS J.* **2010**, *12*, 716−728.

(40) Sullan, R. M.; Li, J. K.; Hao, C.; Walker, G. C.; Zou, S. Cholesterol-Dependent Nanomechanical Stability of Phase-Segregated Multicomponent Lipid Bilayers. *Biophys. J.* **2010**, *99*, 507−516.

(41) Lulevich, V.; Zink, T.; Chen, H. Y.; Liu, F. T.; Liu, G. Y. Cell Mechanics Using Atomic Force Microscopy-Based Single-Cell Compression. *Langmuir* **2006**, *22*, 8151−8155.

(42) Bao, G.; Suresh, S. Cell and Molecular Mechanics of Biological Materials. *Nat. Mater.* **2003**, *2*, 715−725.

(43) Hoffman, B. D.; Crocker, J. C. Cell Mechanics: Dissecting the Physical Responses of Cells to Force. *Annu. Rev. Biomed. Eng.* **2009**, *11*, 259−288.

(44) Lulevich, V.; Shih, Y. P.; Lo, S. H.; Liu, G. Y. Cell Tracing Dyes Significantly Change Single Cell Mechanics. *J. Phys. Chem. B* **2009**, *113*, 6511−6519.

(45) Lulevich, V.; Zimmer, C. C.; Hong, H. S.; Jin, L. W.; Liu, G. Y. Single-Cell Mechanics Provides a Sensitive and Quantitative Means for Probing Amyloid-Beta Peptide and Neuronal Cell Interactions. *Proc. Natl. Acad. Sci. U. S. A.* **2010**, *107*, 13872−13877.

(46) Zimmer, C. C.; Liu, Y. X.; Morgan, J. T.; Yang, G.; Wang, K. H.; Kennedy, I. M.; Barakat, A. I.; Liu, G. Y. New Approach to Investigate the Cytotoxicity of Nanomaterials Using Single Cell Mechanics. *J. Phys. Chem. B* **2014**, *118*, 1246−1255.

(47) Driscoll, K. E.; Costa, D. L.; Hatch, G.; Henderson, R.; Oberdorster, G.; Salem, H.; Schlesinger, R. B. Intratracheal Instillation as an Exposure Technique for the Evaluation of Respiratory Tract Toxicity: Uses and Limitations. *Toxicol. Sci.* **2000**, *55*, 24−35.

(48) Silva, R. M.; Doudrick, K.; Franzi, L. M.; TeeSy, C.; Anderson, D. S.; Wu, Z.; Mitra, S.; Vu, V.; Dutrow, G.; Evans, J. E.; et al. Instillation Versus Inhalation of Multiwalled Carbon Nanotubes: Exposure-Related Health Effects, Clearance, and the Role of Particle Characteristics. *ACS Nano* **2014**, *8*, 8911−8931.

(49) Silva, R. M.; Anderson, D. S.; Franzi, L. M.; Peake, J. L.; Edwards, P. C.; Van Winkle, L. S.; Pinkerton, K. E. Pulmonary Effects of Silver Nanoparticle Size, Coating, and Dose over Time upon Intratracheal Instillation. *Toxicol. Sci.* **2015**, *144*, 151−162.

(50) Anderson, D. S.; Silva, R. M.; Lee, D.; Edwards, P. C.; Sharmah, A.; Guo, T.; Pinkerton, K. E.; Van Winkle, L. S. Persistence of Silver Nanoparticles in the Rat Lung: Influence of Dose, Size, and Chemical Composition. *Nanotoxicology* **2014**, *0*, 1−12.

(51) Wang, X.; Ji, Z.; Chang, C. H.; Zhang, H.; Wang, M.; Liao, Y. P.; Lin, S.; Meng, H.; Li, R.; Sun, B.; et al. Use of Coated Silver Nanoparticles to Understand the Relationship of Particle Dissolution and Bioavailability to Cell and Lung Toxicological Potential. *Small* **2014**, *10*, 385−398.

(52) Bonner, J. C.; Silva, R. M.; Taylor, A. J.; Brown, J. M.; Hilderbrand, S. C.; Castranova, V.; Porter, D.; Elder, A.; Oberdorster, G.; Harkema, J. R.; et al. Interlaboratory Evaluation of Rodent Pulmonary Responses to Engineered Nanomaterials: The Niehs Nano Go Consortium. *Environ. Health Perspect.* **2013**, *121*, 676−682.

(53) Walters, E. H.; Gardiner, P. V. Bronchoalveolar Lavage as a Research Tool. *Thorax* **1991**, *46*, 613−618.

(54) Brown, D. M.; Stone, V.; Findlay, P.; MacNee, W.; Donaldson, K. Increased Inflammation and Intracellular Calcium Caused by Ultrafine Carbon Black is Independent of Transition Metals or Other Soluble Components. *Occup. Environ. Med.* **2000**, *57*, 685−691.

(55) Reynolds, H. Y. Use of Bronchoalveolar Lavage in Humans–Past Necessity and Future Imperative. *Lung* **2000**, *178*, 271−293.

(56) Cleveland, J. P.; Manne, S.; Bocek, D.; Hansma, P. K. A Nondestructive Method for Determining the Spring Constant of Cantilevers for Scanning Force Microscopy. *Rev. Sci. Instrum.* **1993**, *64*, 403−405.

(57) Sader, J. E.; Larson, I.; Mulvaney, P.; White, L. R. Method for the Calibration of Atomic-Force Microscope Cantilevers. *Rev. Sci. Instrum.* **1995**, *66*, 3789−3798.

(58) Lulevich, V.; Yang, H. Y.; Isseroff, R. R.; Liu, G. Y. Single Cell Mechanics of Keratinocyte Cells. *Ultramicroscopy* **2010**, *110*, 1435−1442.

(59) Deng, Z.; Lulevich, V.; Liu, F. T.; Liu, G. Y. Applications of Atomic Force Microscopy in Biophysical Chemistry of Cells. *J. Phys. Chem. B* **2010**, *114*, 5971−5982.

(60) Kang, T.; Lu, W.; Xu, W.; Anderson, L.; Bacanamwo, M.; Thompson, W.; Chen, Y. E.; Liu, D. Microrna-27 (Mir-27) Targets Prohibitin and Impairs Adipocyte Differentiation and Mitochondrial Function in Human Adipose-Derived Stem Cells. *J. Biol. Chem.* **2013**, *288*, 34394−34402.

(61) Tanoue, T.; Takeichi, M. Mammalian Fat1 Cadherin Regulates Actin Dynamics and Cell-Cell Contact. *J. Cell Biol.* **2004**, *165*, 517−528.

(62) Samaj, J.; Baluska, F.; Voigt, B.; Schlicht, M.; Volkmann, D.; Menzel, D. Endocytosis, Actin Cytoskeleton, and Signaling. *Plant Physiol.* **2004**, *135*, 1150−1161.

(63) Oh, N.; Park, J. H. Endocytosis and Exocytosis of Nanoparticles in Mammalian Cells. *Int. J. Nanomed.* **2014**, *9* (Suppl 1), 51−63.

(64) Aderem, A.; Underhill, D. M. Mechanisms of Phagocytosis in Macrophages. *Annu. Rev. Immunol.* **1999**, *17*, 593−623.

(65) Xu, F.; Piett, C.; Farkas, S.; Qazzaz, M.; Syed, N. I. Silver Nanoparticles (Agnps) Cause Degeneration of Cytoskeleton and Disrupt Synaptic Machinery of Cultured Cortical Neurons. *Mol. Brain* **2013**, *6*, 29.

(66) Cheng, X.; Zhang, W.; Ji, Y.; Meng, J.; Guo, H.; Liu, J.; Wu, X.; Xu, H. Revealing Silver Cytotoxicity Using Au Nanorods/Ag Shell Nanostructures: Disrupting Cell Membrane and Causing Apoptosis through Oxidative Damage. *RSC Adv.* **2013**, *3*, 2296−2305.

(67) Manke, A.; Wang, L.; Rojanasakul, Y. Mechanisms of Nanoparticle-Induced Oxidative Stress and Toxicity. *BioMed Res. Int.* **2013**, *2013*, 942916.

(68) Forman, H. J.; Torres, M. Reactive Oxygen Species and Cell Signaling: Respiratory Burst in Macrophage Signaling. *Am. J. Respir. Crit. Care Med.* **2002**, *166*, S4−8.

(69) Zhang, T.; Wang, L.; Chen, Q.; Chen, C. Cytotoxic Potential of Silver Nanoparticles. *Yonsei Med. J.* **2014**, *55*, 283−291.

(70) Nel, A. E.; Madler, L.; Velegol, D.; Xia, T.; Hoek, E. M. V.; Somasundaran, P.; Klaessig, F.; Castranova, V.; Thompson, M. Understanding Biophysicochemical Interactions at the Nano-Bio Interface. *Nat. Mater.* **2009**, *8*, 543−557.

(71) Loza, K.; Diendorf, J.; Sengstock, C.; Ruiz-Gonzalez, L.; Gonzalez-Calbet, J. M.; Vallet-Regi, M.; Koller, M.; Epple, M. The Dissolution and Biological Effects of Silver Nanoparticles in Biological Media. *J. Mater. Chem. B* **2014**, *2*, 1634−1643.

(72) Kone, B. C.; Kaleta, M.; Gullans, S. R. Silver Ion (Ag+)-Induced Increases in Cell Membrane K+ and Na+ Permeability in the Renal Proximal Tubule: Reversal by Thiol Reagents. *J. Membr. Biol.* **1988**, *102*, 11−19.

(73) He, D.; Jones, A. M.; Garg, S.; Pham, A. N.; Waite, T. D. Silver Nanoparticle-Reactive Oxygen Species Interactions: Application of a Charging-Discharging Model. *J. Phys. Chem. C* **2011**, *115*, 5461−5468.